Electronic Supplementary Material (ESI) for Dalton Transactions.

Supplementary data

Methanolysis of Ammonia Borane by Shape-Controlled Mesoporous Copper Nanostructures for Hydrogen Generation

Qilu Yao,[a#] Ming Huang,[b#] Zhang-Hui Lu,[a*] Yuwen Yang,[a] Yuxin Zhang,[b*] Xiangshu Chen,[a*] Zhen Yang[a]

[a]*Jiangxi Inorganic Membrane Materials Engineering Research Centre, College of Chemistry and Chemical Engineering, Jiangxi Normal University, Nanchang, 330022, China;* [b]*College of Materials Science and Engineering, Chongqing University, Chongqing 400044, China*

* E-mail address: luzh@jxnu.edu.cn (Z.–H. Lu), zhangyuxin@cqu.edu.cn (Y.X. Zhang), cxs66cn@jxnu.edu.cn (X. Chen).

Experimental Section

Synthesis of mesoporous CuO with diverse shapes

Mesoporous CuO nanostructures with diverse shapes were prepared via a facile and scaleable wet-chemical method.[40,41]

Flower- and bundle-like mesoporous CuO nanostructures

In brief, an aqueous $Cu(NO_3)_2{\cdot}3H_2O$ solution (20 mL, 0.05 M) was mixed with TOAB ethanol solution (40 mL, 0.05 M) in a round-bottom flask. After vigorous stirring at room temperature for 5 min, different amount (4 mL for bundle-like, 8 mL flower-like) of $NH_3{\cdot}H_2O$ (25-28 %) was injected quickly. And then aqueous solution of NaOH (10 mL, 1.00 M) was dropwisely added into the mixture with vigorous stirring for 1.5 h. The resulting dark blue precipitates were separated, centrifuged, washed with distilled water and ethanol for several times, and dried at 333 K in vacuum, giving the intermediate products. Finally, the different shapes of CuO were obtained by calcining the intermediate products at 773 K in air for 1 h.

Nanosheets-like mesoporous CuO nanostructures

An aqueous $Cu(NO_3)_2{\cdot}3H_2O$ solution (20 mL, 0.05 M) was mixed with TOAB ethanol solution (40 mL, 0.05 M) in a round-bottom flask. After vigorous stirring at 60 ^oC in water bath for 5 min, 6 mL of $NH_3{\cdot}H_2O$ (25-28 %) was injected quickly. And then aqueous solution of NaOH (10 mL, 1.00 M) was dropwisely added into the mixture with vigorous stirring for 1.5 h. The resulting dark precipitates were separated, centrifuged, washed with distilled water and ethanol for several times, and dried at 60 ^oC in vacuum, giving the intermediate products. Finally, CuO nanosheets were obtained by calcining the intermediate products at 773 K in air for 1 h.

Dandelion-like mesoporous CuO nanostructures

$Cu(NO_3)_2{\cdot}3H_2O$ ethanol solution (15 mL, 0.1 M) was mixed with $NH_3{\cdot}H_2O$ (15 ml, 25-28%), and then 5 mL NaOH (1.0 M) was added to the mixture. After stirring for 10 min to form a clear solution, the resulting solution was transferred into a 50 mL stainless-steel autoclaves lined with poly(tetrafluoroethylene) (PTFE, Telfon). The autoclave was closed and heated at 453 K for 5 h and then cooled down to room temperature. The resulting precipitate solid were collected by centrifugation, washed with distilled water and absolute ethanol, and finally dried at 333 K.

Powder X-ray diffraction (XRD) was performed on the as-synthesized mesoporous CuO NPs with flower-, nanosheets-, bundle-, and dandelion-like shapes. As shown in Fig. S1, the positions of diffraction peaks indicate that these samples are crystallite phase with monoclinic CuO matched the JCPDS card no. 45-0937 (*a* = 4.685 Å, *b* = 3.426 Å, *c* =5.13 Å and *β* = 99.55°), similar to our previous reports.[40,41] No other diffraction peaks can be detected, indicating that the as-prepared mesoporous CuO are high purity.

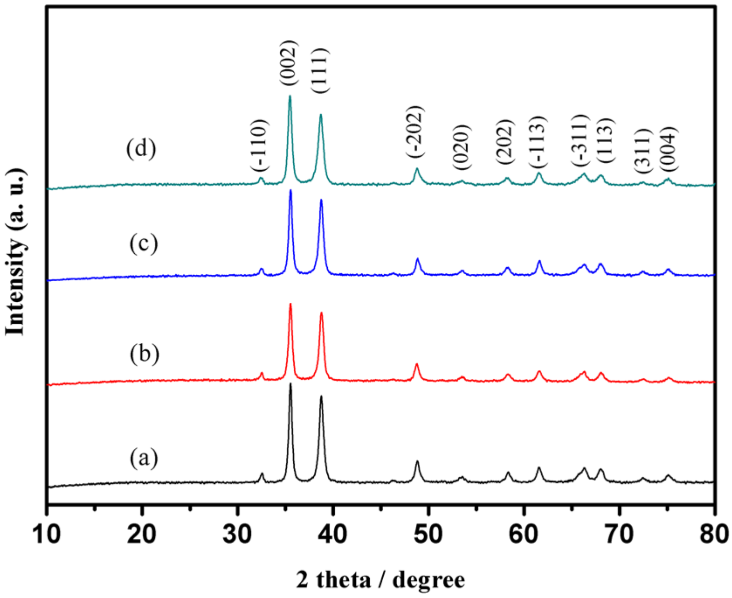

Fig. S1 Powder X-ray diffraction patterns of the as-synthesized mesoporous CuO nanostructures with a) flower-like, b) nanosheets-like, c) bundle-like, and d) dandelion-like shape.

SEM measurements were performed on the as-synthesized nanostructured mesoporous CuO with diverse morphologies (flower-like, nanosheets-like, bundle-like and dandelion-like CuO). As shown in Fig. S2a, the morphology of the CuO is flower-like, with a diameter ranging from 4 to 5 μm and the nanobranches with average widths of 5 to 10 nm. Fig. S2b reveals that the size of nanosheets-like CuO is 60 nm in thickness and 600 nm in width. The width and length of the bundle-like CuO particles are about 100~300 nm and 0.4~1 μm, respectively (Fig. S2c). The diameter of dandelion-like CuO is about 3~5 μm, and self-assembly of nanoplates with an average thickness of about 10-20 nm (Fig. S2d).

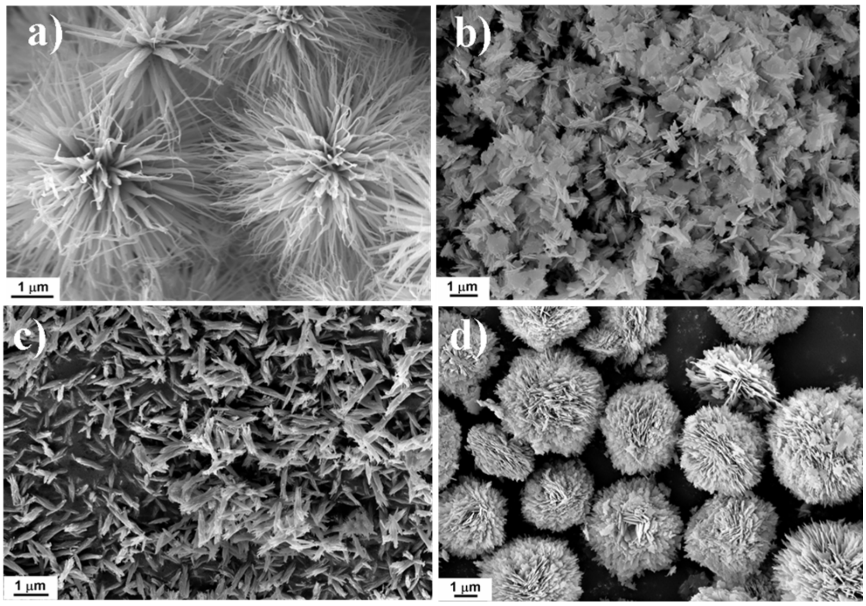

Fig. S2 SEM images of the as-synthesized mesoporous CuO anostructures with a) flower-like, b) nanosheets-like, c) bundle-like, and d) dandelion-like shape.

The nitrogen physisorptions were investigated for the as-synthesized mesoporous CuO nanostructures with different morphologies. From the corresponding nitrogen adsorption-desorption isotherms (Fig. S3), we can see that the CuO samples exhibit similar curve shapes. The typical IV isotherms with a hysteresis loop occur at a relative pressure of 0.8-0.95 (Fig. S3), showing the existence of mesopores in all the as-synthesized mesoporous CuO, which is further confirmed by the pore diameters (11.1~22.6 nm) of the samples (Table S1). The BET surface area, pore diameter, and pore volume of as-synthesized mesoporous CuO are listed in Table S1.

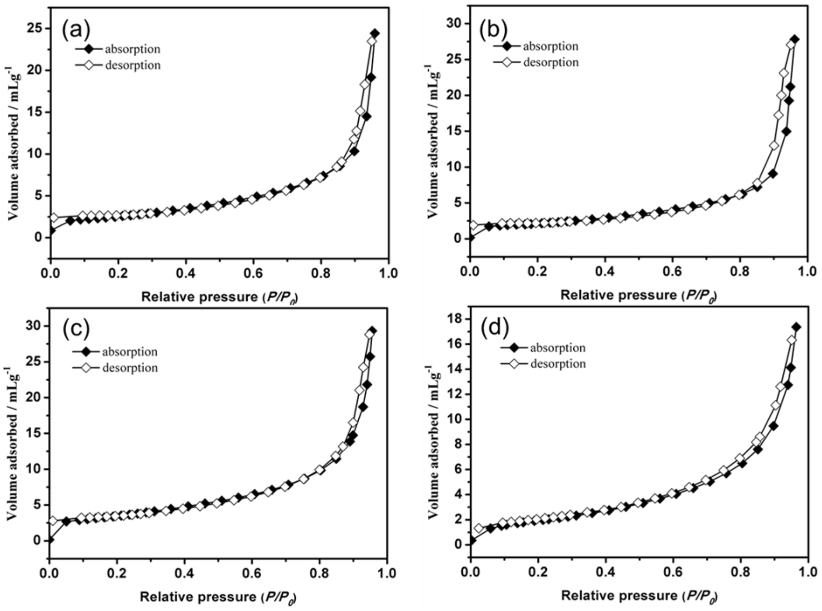

Fig. S3 Nitrogen adsorption-desorption isotherms of the as-synthesized mesoporous CuO nanostructures with a) flower-like, b) nanosheets-like, c) bundle-like, and d) dandelion-like shape.

Table S1 BET Surface area, pore diameter and pore volume of the as-synthesized CuO with diverse morphologies.

Catalyst	BET surface area (m^2 g^{-1})	Pore size (nm)	Pore volume (cm^3 g^{-1})
Flower-like CuO	9.08	16.62	0.038
Nanosheets-like CuO	12.50	11.13	0.045
Bundle-like CuO	7.62	22.58	0.042
Dandelion-like CuO	11.30	11.83	0.031

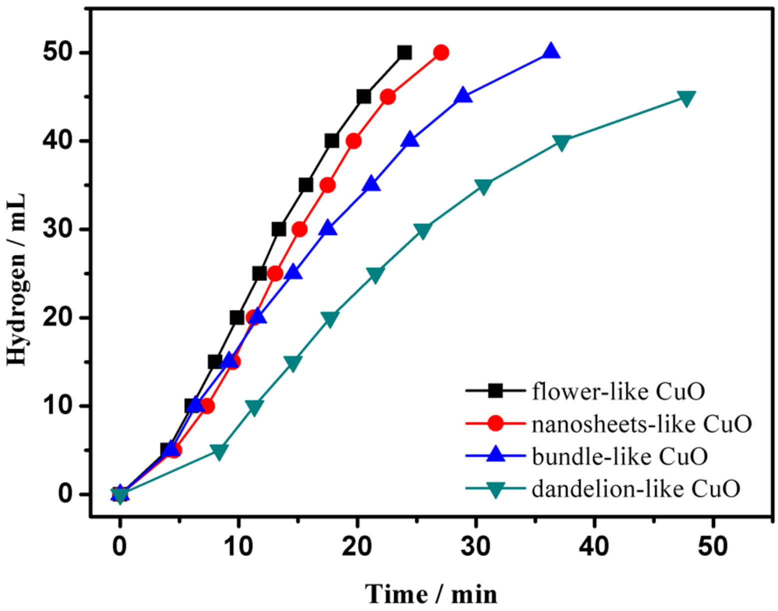

Fig. S4 The as-synthesized mesoporous CuO nanostructures reduced by NH_3BH_3 (0.2 M, 5 mL) at 298 K ($Cu/NH_3BH_3 = 0.15$).

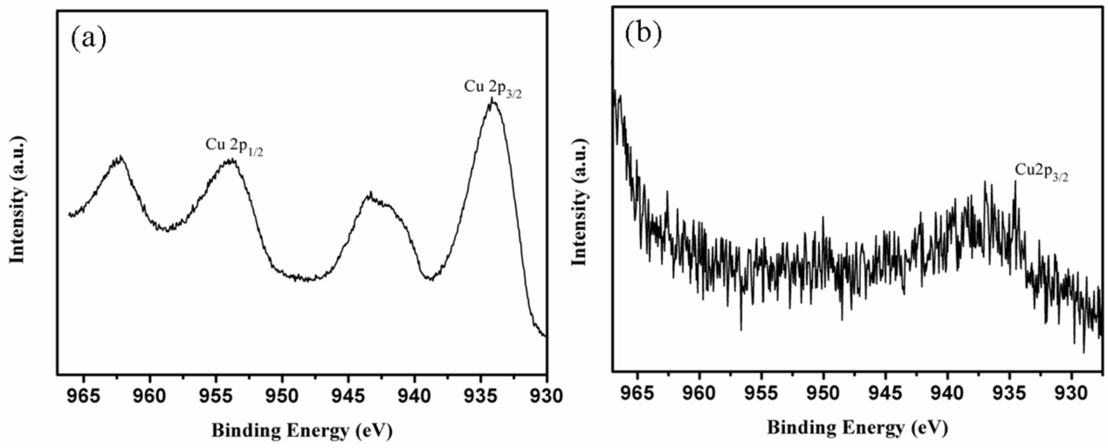

Fig. S5 X-Ray photoelectron spectra of the flower-like mesoporous (a) CuO (b) Cu nanostructures.

Table S2 BET Surface area, pore diameter and pore volume of the mesoporous Cu before the methanolysis of NH_3BH_3.

Catalyst	BET surface area (m^2 g^{-1})	Pore size (nm)	Pore volume (cm^3 g^{-1})
Flower-like Cu	7.39	12.13	0.022
Nanosheets-like Cu	9.44	10.68	0.025
Bundle-like Cu	6.20	11.83	0.018
Dandelion-like Cu	7.28	14.75	0.027

Compared to the samples of the as-synthesized CuO (Table S1), the BET surface area, pore diameter, and pore volume of mesoporous Cu show a decrease after reduction reaction, which is due to that CuO were reduced to Cu by AB during the methanolysis reaction.

Table S3 Reactive surface area of the mesoporous Cu before the methanolysis of NH_3BH_3.

Catalyst	Reactive surface area (m^2 g^{-1})
Flower-like Cu	2.67
Nanosheets-like Cu	2.06
Bundle-like Cu	1.02
Dandelion-like Cu	0.91

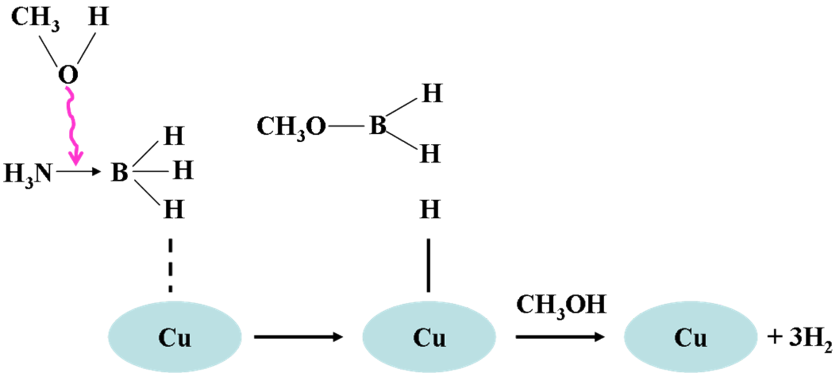

Fig. S6 Plausible mechanism of mesoporous Cu nanostructures for hydrogen generation from the methanolysis of NH_3BH_3.

Table S4 TOF values (mol H_2 mol catalyst^{-1} min^{-1}) of Cu nanocatalysts tested in hydrogen generation from AB in methanolysis or hydrolysis reaction.

Catalyst	**TOF (**mol H_2 mol catalyst^{-1} min^{-1})	**Ref.**
Cu/RGO^b	3.61	27
Flower-like Cu^a	2.41	This study
Zeolite-confined Cu^b	1.25	43
p(AMPS)-Cu^b	0.72	44
Cu/γ-Al_2O_3^{b}	0.27	45
$CuCl_2$^{b}	0.23	46
Cu_2O^{a}	0.20	47
Cu^a	0.07	47

Note: ^{a}Hydrogen generation from AB in methanolysis

^{b}Hydrogen generation from AB in hydrolysis.

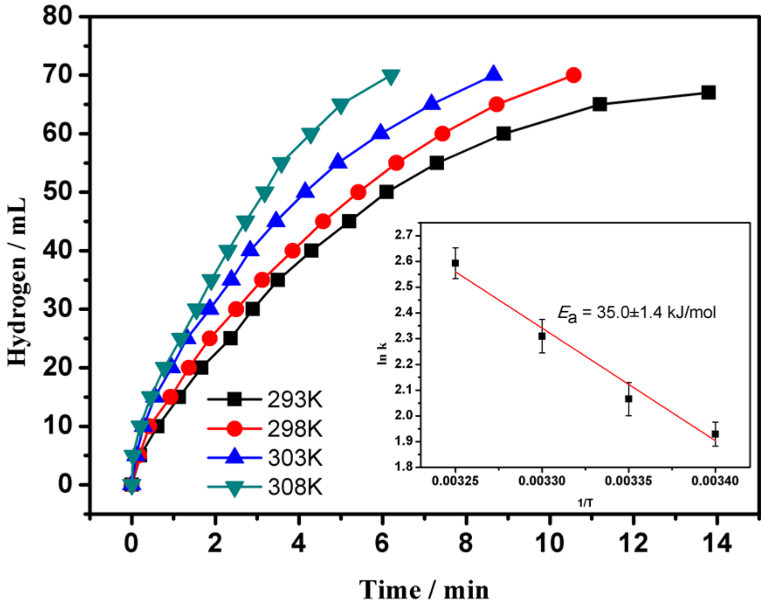

Fig. S7 Hydrogen generation from the methanolysis of NH_3BH_3 (0.2 M, 5 mL) in the presence of nanosheets-like Cu at 293-308 K ($Cu/NH_3BH_3 = 0.15$). The inset shows the Arrhenius plot (ln k vs. 1/T).

We have chosen three different ranges (0-50 mL, 10-50 mL and 20-50 mL), and given the activity plot and activation energies with standard deviation bars.

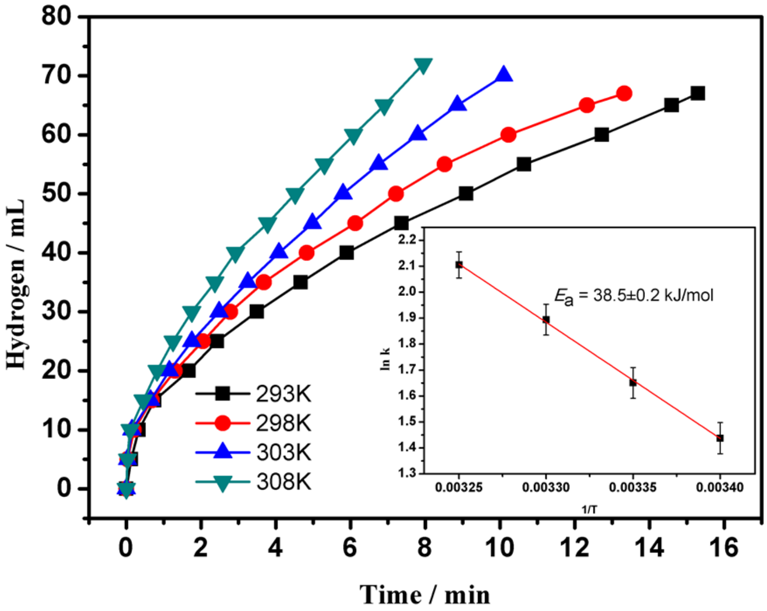

Fig. S8 Hydrogen generation from the methanolysis of NH_3BH_3 (0.2 M, 5 mL) in the presence of bundle-like Cu at 293-308 K (Cu/NH_3BH_3 = 0.15). The inset shows the Arrhenius plot (ln k vs. 1/T).

We have chosen three different ranges (0-50 mL, 10-50 mL and 20-50 mL), and given the activity plot and activation energies with standard deviation bars.

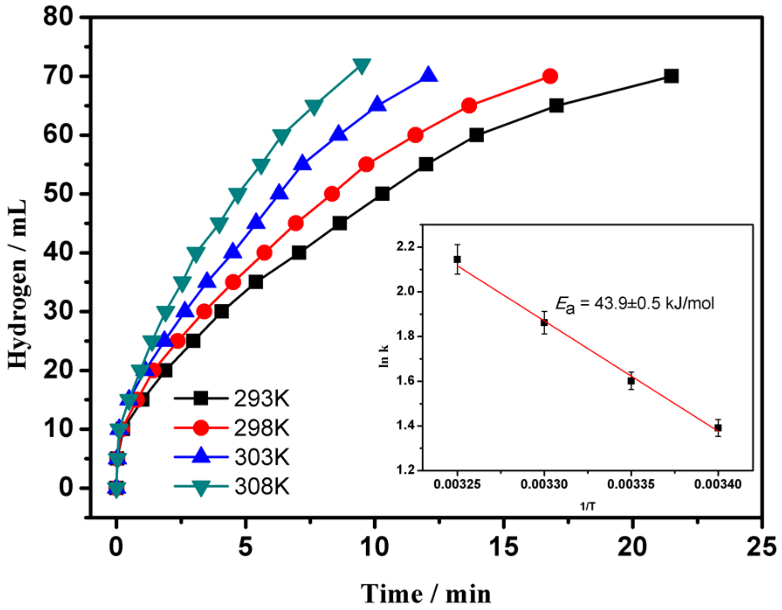

Fig. S9 Hydrogen generation from the methanolysis of NH_3BH_3 (0.2 M, 5 mL) in the presence of dandelion-like Cu at 293-308 K. The inset shows the Arrhenius plot (ln k vs. 1/T).

We have chosen three different ranges (0-50 mL, 10-50 mL and 20-50 mL), and given the activity plot and activation energies with standard deviation bars.

Table S5 The values of activation energy (E_a) of catalysts reported in hydrogen generation from AB in solvolysis.

Catalyst	**E_a (kJ mol^{-1})**	**Ref.**
Ru/carbon^b	76	S1
Co/γ-Al_2O_3^{b}	62	45
Ru/Hydroxyapatite^b	58	S2
PVP stabilized Ru(0)^a	58	36
Pd-PVP-TiO_2^{b}	55	S3
Pd/Hydroxyapatite^b	54.8 ± 2	S4
PSSA-co-MA stabilized Ru^b	54	S5
p(AMPS)-Ni^b	52.8	44
Zeolite-confined Cu^b	51.8 ± 1.8	43
Ru/carbon black (CB)^b	49.18	S6
p(AMPS)-Cu^b	48.8	44
Zeolite stabilized Rh^a	40 ± 2	37
Cu/RGO^b	38.2 ± 1.5	27
PVP-stabilized Pd(0)^a	35 ± 2	35
Ru/C^b	34.81 ± 0.12	S7
Flower-like Cu^a	34.2 ± 1.2	This study
Ru/montmorillonite^a	23.8 ± 1.2	38

[a] Hydrogen generation from AB in methanolysis

[b] Hydrogen generation from AB in hydrolysis

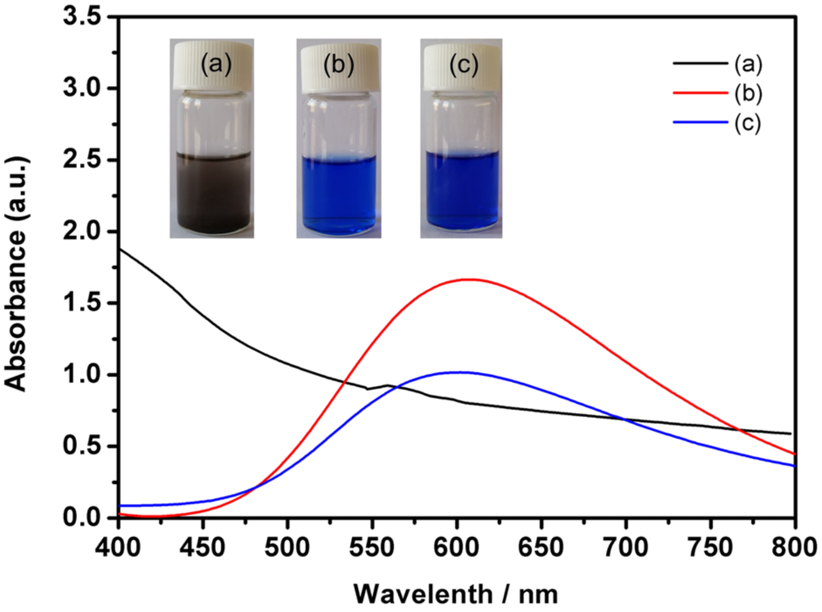

Fig. S10 UV-Vis spectra of (a) Cu NPs, (b) the solution after oxidative etching of Cu NPs in air and (c) the filtrate after removing Cu catalysts with addition of $CuCl_2$.

The black suspension containing Cu NPs after the first reaction was stirred in air. 20 min later, the black suspension was changed into the blue solution. Then, another equivalent of AB was subsequently added into the blue solution to get the black Cu NPs again, and the recycle activity of the regenerated Cu NPs to methanolysis of AB was tested. UV-Vis absorption spectroscopy was carried out to monitor the above conversion (Fig. S10). As shown in Fig. S10a, the broad absorption peak of at ~560 nm were assigned to Cu NPs. After the reaction, the suspension changes its black color to blue within 20 min and shows a broad absorption peak of at ~600 nm (Fig. S10b), which implies that Cu NPs are returned to Cu^{2+} cations. To confirm this assumption, Cu NPs were separated away from the reaction solution after the reaction. Then, $CuCl_2$ was added into the filtrate. The filtrate with $CuCl_2$ was used for UV-Vis analysis. As shown in Fig. S10c, the similar broad absorption peak of at ~600 nm were observed as those of the solution after oxidative etching of Cu NPs in air (Fig. S10b). This means that Cu NPs are transformed into Cu^{2+} cations after oxidative etching of Cu NPs in the reaction solution. The reactions were repeated for five times under ambient atmosphere at room temperature. The catalyst retains 93% of its initial catalytic activity after the fifth run methanolysis of AB. The regenerated Cu NPs maintain their high catalytic activity for AB methanolysis. A similar phenomenon has also been observed for Co catalysts by Wang and co-workers (See: J. Power Sources, 2013, 243, 431).

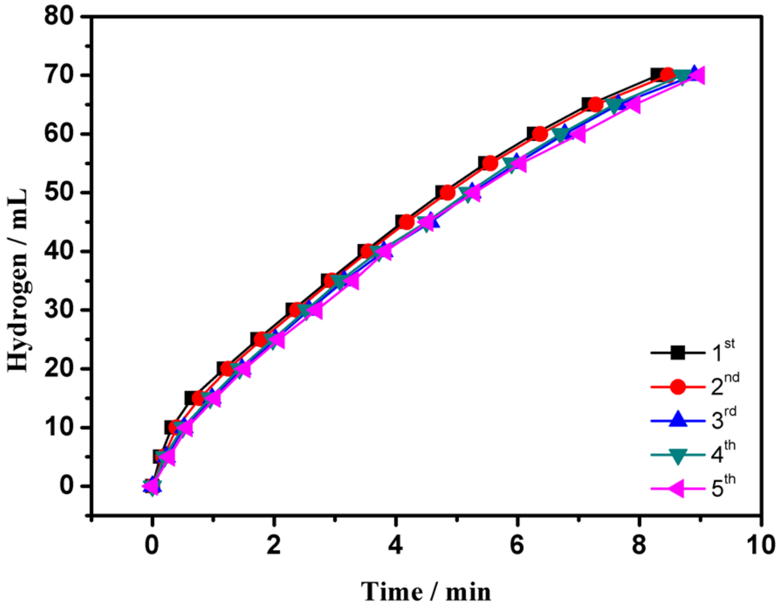

Fig. S11 Hydrogen generation from the methanolysis of NH_3BH_3 (0.2 M, 5 mL) in the presence of flower-like Cu at 298 K in sequential runs ($Cu/NH_3BH_3 = 0.15$).

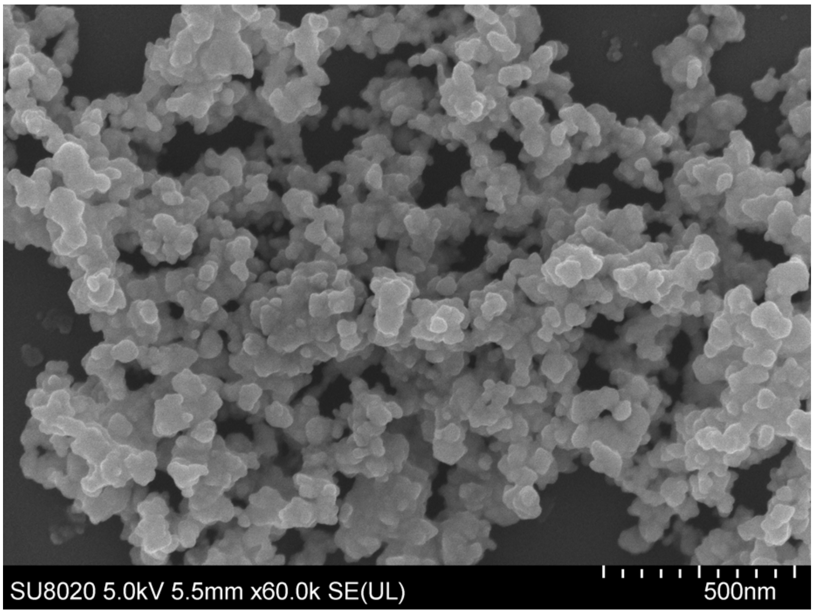

Fig. S12 SEM image of the flower-like Cu nanostructures after five runs of methanolysis of NH_3BH_3.

References

S1. S. Basu, A. Brockman, P. Gagare, Y. Zheng and P. V. Ramachandran, *J. Power Sources*, 2009, **188**, 238.

S2. S. Akbayrak, P. Erdek and S. Özkar, *Appl. Catal. B-Environ.*, 2013, **142** 187.

S3. M. Rakap, E. E. Kalu and S. Özkar, *Int. J. Hydrogen Energy*, 2011, **6**, 448.

S4. M. Rakap and S. Özkar, *Int. J. Hydrogen Energy*, 2011, **36**, 7019.

S5. Ö. Metin, Ş. Şahin and S. Özkar, *Int. J. Hydrogen Energy*, 2009, **34**, 6304.

S6. G. Z. Chen, S. Desinan, R. Rosei, F. Rosei and D. L. Ma, *Chem. Eur. J.*, 2012, **18**, 7925.

S7. H. Y. Liang, G. Z. Chen, S. Desinan, R. Rosei, F. Rosei and D. L. Ma, *Int. J. Hydrogen Energy*, 2012, **37**, 17921.